Spectral Image of Human Portrait

Qun Sun, Mark D. Fairchild

Munsell Color Science Laboratory
Chester F. Carlson Center for Imaging Science
Rochester Institute of Technology
54 Lomb Memorial Dr.
Rochester, NY 14623-5604

Abstract

This report describes the procedure of capturing spectral images of human portraits. The spectral reflectances of human faces, including hair, eyes and lips, are analyzed by principal component analysis (PCA). Reconstructed spectral images based on the first three and six principal components are calculated. The results indicate that three basis functions are accurate enough to estimate the spectral reflectance of human faces. Due to the image quality limitation of the camera, spectral images based on six basis functions involve relatively large noise. The derived spectral images can be applied to color-imaging system design and analysis.

Introduction

Most of the traditional color-imaging and reproduction systems functioned in a trichromatic fashion with three response functions, resulting in three color signals, i.e., RGB color values. These approaches could reproduce color quite capably. However, there are several problems inherent in these approaches, which will cause large color shifts. This becomes apparent in the image capture and reproduction of metameric objects[1]. The only way to solve these problems is to attempt to produce spectral matches between the original objects and their reproductions. The key idea is to replace the world of red, green and blue with the world of wavelength[2]. The study of spectral imaging of pictorial scenes in this report is motivated in part by the previous multi-spectral imaging-research of artwork[3, 4, 5, 6, 7] and realistic spectral image synthesis [1] in the Munsell Color Science Laboratory, and spectral skin color image research by Imai et al.[8,]. They

provide formulation and method involving spectral imaging system and spectral image capture. They also provide a detail study of spectral image application in human skin and computer graphics. Previous research [8, 9], based on 108 reflectance spectra of skin in faces of 54 Japanese women, showed that the spectral reflectance of human skin, can be represented by three basis functions using PCA. Therefore, the spectral reflectance of each pixel of the captured image could be estimated from the values of three color channels and the spectral radiance of the illuminant used. However, a high quality spectral human portrait needs some specific consideration of its own. Generally, previous spectral portrait image researches [8, 9] performed the system calibration based on the painting samples which were the reproductions of the reflectance spectra of skin directly measured. These approaches required very accurate reproductions of skin at a fairly early stage to avoid the errors passed through all the following procedures. Moreover, those reproduced spectral paintings excluded the spectra of the lips, eyes and hairs which we consider are important parts of the human portrait information. On the other hand, for spectral reflectance of the human face, different measurement geometry will give different spectral information. In the real world, the spectral reflectance of human face captured by the camera or detector is a mixture of diffuse reflection, specular reflections and interreflections. Therefore, we believe that the spectral reflectance of human face based on direct measurement, i. e., putting spectrophotometer on the face to measure the spectral reflectance, could not contain the geometric spectral information related to the certain objects under certain lighting conditions. Consequently, the basis functions derived from principal component analysis, based on the spectra which are directly measured from painting targets or real objects, and their further application are not precise. Other researchers [10] calibrated their system and determined basis functions based on Munsell chips, paint chips and natural objects. We consider those methods could neither provide sufficient geometric information of the real spectral reflectance of the face nor represent them precisely. This research will perform efforts to calibrate the imaging system and capture spectral images of human portrait based on the spectral data directly recorded from the real objects with certain lighting and camera conditions. The detail of the experiment procedure will be provided. The calibrated imaging system will have the ability to represent either the face skin or the spectra of lips, eyes and hairs as

well. The spectral reflectance measured above will be analyzed by PCA. Based on the results of PCA, both three wide band and six wide band spectral images will be estimated respectively. The detail of the estimation procedure will be provided. The results of the reconstructed spectral images for display based on sRGB model will be shown and discussed.

Model of Spectral Image

Multi-spectral image acquisition can be modeled using matrix-vector notation [11]. The illumination spectral power distribution can be expressed as

$$\mathbf{S} = \begin{bmatrix} s_1 & & 0 \\ & s_2 & \\ & & \ddots \\ 0 & & s_n \end{bmatrix}, \quad (1)$$

where the index indicates the set of n wavelengths over the visible range. The object spectral reflectance can be expressed as $\mathbf{r} = [r_1, r_2, ..., r_n]^T$ where T means matrix transpose. The transmittance characteristics of the m filters (in our case m =3, 6 respectively) will be the following form:

$$\mathbf{F} = \begin{bmatrix} f_1 & f_{1,2} & \cdots & f_{1,m} \\ \vdots & \vdots & \cdots & \vdots \\ f_{n,1} & f_{n,2} & \cdots & f_{n,m} \end{bmatrix} \quad (2)$$

The spectral sensitivity of the detector, i.e., camera, will be given as:

$$\mathbf{D} = \begin{bmatrix} d_1 & & 0 \\ & d_2 & \\ & & \ddots \\ 0 & & d_n \end{bmatrix}. \quad (3)$$

Then the captured image is given by

$$\mathbf{I} = (\mathbf{D}\ \ \mathbf{F})^{T}\ \ \mathbf{S}\ \ \mathbf{r} = \begin{bmatrix} \sum_{l=1}^{n} f_{l,1}\ \ d_l\ \ s_l\ \ r_l \\ \sum_{l=1}^{n} f_{l,2}\ \ d_l\ \ s_l\ \ r_l \\ \vdots \\ \sum_{l=1}^{n} f_{l,m}\ \ d_l\ \ s_l\ \ r_l \end{bmatrix}, \tag{4}$$

where **I** is the digital counts of the pixel. The spectral reflectance of each pixel, theoretically, can be obtained using pseudoinverse from Eq.(4). However, in our case, there are only six digital counts for each pixel, the spectral reflectance obtained using pseudoinverse method here may yield large uncertainty and give large error. The advantage here, as authors understand [12], is convenient to do simulation and check the results. Therefore, PCA method will be performed as an alternative choice. We will discuss this in detail below. The color vector can be obtained as $\mathbf{C} = \mathbf{A}\cdot\mathbf{I} = (X,Y,Z)^{T}$ where X, Y, Z are the CIE tristimulus values and A is a transfer matrix. The CIELab L*, a*, b* are given by the non-linear transformation Ψ, where Ψ(X,Y,Z) = L*, a*, b*.

The spectral reflectance R(x, y, λ), where x, y denote the coordinates of the image pixel, can be estimated using spectral reconstruction methods based on statistical analyses, PCA. It can also be obtained by using interpolation techniques such as cubic spline done by Burns [11]. Burns and Berns[13] indicated that the method of PCA would give more accurate results than interpolation methods.

The PCA method is a mathematical technique which describes a multivariate set of measured data using basis functions, or called eigenvectors. The basis functions are formulated using specific linear combinations of the original variables. The basis functions are uncorrelated and are computed in decreasing order of importance; the first function accounts for as much as possible of the variation in the original data, the second function accounts for the second largest portion of the variation in the original data, and so on. The PCA method attempts to construct a small set of basis functions which summarize the original data, thereby reducing the dimensionality of the original data. In practice, though the accuracy of spectral reconstruction depends on the number of basis functions used, 5 to 8 basis functions are sufficient for accurate spectral reconstruction

used in artwork[14], while 3 basis functions are satisfied in spectral reproduction of human skin[8]. Details of the PCA can be found in many textbooks[15, 16].

Applying the PCA method to the measured spectral reflectance of the objects, the number of basis functions for accurate spectral reproduction can be determined based on the cumulative proportion rates of the basis functions. Suppose six basis functions are sufficient to represent the spectral reflectance of human face, including skin, hairs, eyes and lips. The spectral reflectance of human face can then be expressed as a linear combination of the basis functions as follows: where $\bar{\mathbf{r}}$ is the average spectral

$$\mathbf{r} = \bar{\mathbf{r}} + \sum_{i=1}^{6} \alpha_i \mathbf{u}_i = \bar{\mathbf{r}} + (\mathbf{u}_1\ \mathbf{u}_2\ \mathbf{u}_3\ \mathbf{u}_4\ \mathbf{u}_5\ \mathbf{u}_6)\begin{pmatrix}\alpha_1\\ \alpha_2\\ \alpha_3\\ \alpha_4\\ \alpha_5\\ \alpha_6\end{pmatrix}, \tag{5}$$

reflectance, $\mathbf{u}_i$ are the basis functions, or eigenvectors, and α_i are the eigenvalues. The tristimulus values X, Y, Z can be calculated by Eq. (6):

$$\begin{aligned} X &= K \sum_{\lambda=380}^{780} E(\lambda)\ \overline{x(\lambda)}\ r(\lambda), \\ Y &= K \sum_{\lambda=380}^{780} E(\lambda)\ \overline{y(\lambda)}\ r(\lambda), \\ Z &= K \sum_{\lambda=380}^{780} E(\lambda)\ \overline{z(\lambda)}\ r(\lambda), \end{aligned} \tag{6}$$

where r(λ) is the spectral reflectance, E(λ) is the spectral radiance of the illumination, $\overline{x(\lambda)}$, $\overline{y(\lambda)}$, $\overline{z(\lambda)}$ are the color matching functions, and K is a normalized constant. Eq. (6) can be converted to matrix notation as follows:

$$\begin{aligned} X &= K\mathbf{e}^T\bar{\mathbf{x}}\mathbf{r}, \\ Y &= K\mathbf{e}^T\bar{\mathbf{y}}\mathbf{r}, \\ Z &= K\mathbf{e}^T\bar{\mathbf{z}}\mathbf{r}, \end{aligned} \tag{7}$$

where T represent the transpose, the matrix **e** and **r** are matrix notations of E(λ) and r(λ) respectively. And the matrices $\bar{\mathbf{x}}, \bar{\mathbf{y}}, \bar{\mathbf{z}}$ are color-matching function represented as follows:

$$\bar{\mathbf{x}} = \begin{bmatrix} \bar{x}_1 & & 0 \\ & \bar{x}_2 & \\ & & \ddots \\ 0 & & \bar{x}_n \end{bmatrix}, \tag{8}$$

$$\bar{\mathbf{y}} = \begin{bmatrix} \bar{y}_1 & & 0 \\ & \bar{y}_2 & \\ & & \ddots \\ 0 & & \bar{y}_n \end{bmatrix}, \tag{9}$$

$$\bar{\mathbf{z}} = \begin{bmatrix} \bar{z}_1 & & 0 \\ & \bar{z}_2 & \\ & & \ddots \\ 0 & & \bar{z}_n \end{bmatrix}. \tag{10}$$

From Eq. (5), Eq. (7) can be written as

$$X = K\mathbf{e}^T \bar{\mathbf{x}} \bar{\mathbf{r}} + (\mathbf{u}_1\, \mathbf{u}_2\, \mathbf{u}_3\, \mathbf{u}_4\, \mathbf{u}_5\, \mathbf{u}_6) \begin{bmatrix} \alpha_1 \\ \alpha_2 \\ \alpha_3 \\ \alpha_4 \\ \alpha_5 \\ \alpha_6 \end{bmatrix} \tag{11}$$

$$Y = K\mathbf{e}^T \bar{\mathbf{y}} \bar{\mathbf{r}} + (\mathbf{u}_1\, \mathbf{u}_2\, \mathbf{u}_3\, \mathbf{u}_4\, \mathbf{u}_5\, \mathbf{u}_6) \begin{bmatrix} \alpha_1 \\ \alpha_2 \\ \alpha_3 \\ \alpha_4 \\ \alpha_5 \\ \alpha_6 \end{bmatrix} \tag{12}$$

$$Z = K\mathbf{e}^T \bar{\mathbf{z}} \begin{bmatrix} \bar{r} \\ \bar{r} \\ \bar{r} \\ \bar{r} \\ \bar{r} \\ \bar{r} \end{bmatrix} + (\mathbf{u}_1\ \mathbf{u}_2\ \mathbf{u}_3\ \mathbf{u}_4\ \mathbf{u}_5\ \mathbf{u}_6) \begin{bmatrix} \alpha_1 \\ \alpha_2 \\ \alpha_3 \\ \alpha_4 \\ \alpha_5 \\ \alpha_6 \end{bmatrix}. \tag{13}$$

Eq. (11) ~(13) then can be rewritten as follows:

$$X = K\mathbf{e}^T \bar{\mathbf{x}} \begin{bmatrix} \bar{r} \\ \bar{r} \\ \bar{r} \\ \bar{r} \\ \bar{r} \\ \bar{r} \end{bmatrix} + K\mathbf{e}^T (\bar{x}\mathbf{u}_1\ \bar{x}\mathbf{u}_2\ \bar{x}\mathbf{u}_3\ \bar{x}\mathbf{u}_4\ \bar{x}\mathbf{u}_5\ \bar{x}\mathbf{u}_6) \begin{bmatrix} \alpha_1 \\ \alpha_2 \\ \alpha_3 \\ \alpha_4 \\ \alpha_5 \\ \alpha_6 \end{bmatrix}, \tag{14}$$

$$Y = K\mathbf{e}^T \bar{\mathbf{y}} \begin{bmatrix} \bar{r} \\ \bar{r} \\ \bar{r} \\ \bar{r} \\ \bar{r} \\ \bar{r} \end{bmatrix} + K\mathbf{e}^T (\bar{y}\mathbf{u}_1\ \bar{y}\mathbf{u}_2\ \bar{y}\mathbf{u}_3\ \bar{y}\mathbf{u}_4\ \bar{y}\mathbf{u}_5\ \bar{y}\mathbf{u}_6) \begin{bmatrix} \alpha_1 \\ \alpha_2 \\ \alpha_3 \\ \alpha_4 \\ \alpha_5 \\ \alpha_6 \end{bmatrix}, \tag{15}$$

$$Z = K\mathbf{e}^T \bar{\mathbf{z}} \begin{bmatrix} \bar{r} \\ \bar{r} \\ \bar{r} \\ \bar{r} \\ \bar{r} \\ \bar{r} \end{bmatrix} + K\mathbf{e}^T (\bar{z}\mathbf{u}_1\ \bar{z}\mathbf{u}_2\ \bar{z}\mathbf{u}_3\ \bar{z}\mathbf{u}_4\ \bar{z}\mathbf{u}_5\ \bar{z}\mathbf{u}_6) \begin{bmatrix} \alpha_1 \\ \alpha_2 \\ \alpha_3 \\ \alpha_4 \\ \alpha_5 \\ \alpha_6 \end{bmatrix}. \tag{16}$$

We can treat the first terms of Eqs. (14)~(16) as the contribution of the averaged spectral reflectance to the tristimulus values, and the second terms as the contribution of six basis functions or eigenvectors. Therefore, we have the following equation:

$$\begin{bmatrix} X \\ Y \\ Z \end{bmatrix} = \begin{bmatrix} \bar{X} \\ \bar{Y} \\ \bar{Z} \end{bmatrix} + \begin{bmatrix} X_1 & X_2 & X_3 & X_4 & X_5 & X_6 \\ Y_1 & Y_2 & Y_3 & Y_4 & Y_5 & Y_6 \\ Z_1 & Z_2 & Z_3 & Z_4 & Z_5 & Z_6 \end{bmatrix} \begin{bmatrix} \alpha_1 \\ \alpha_2 \\ \alpha_3 \\ \alpha_4 \\ \alpha_5 \\ \alpha_6 \end{bmatrix} \tag{17}$$

where $\overline{X}, \overline{Y}, \overline{Z}$ are the averaged tristimulus values and X_i, Y_i, Z_i(i = 1,2,...,6) are the tristimulus values corresponding to the six basis functions of spectral reflectance of face. However, to determine the six eigenvalues, three more equations need to be provided. Therefore, a filter is employed, either in front of the lighting source or detector, to yield another three equations as follows:

$$\begin{aligned} X_f &= K \sum_{\lambda=380}^{780} E(\lambda)\ \overline{x(\lambda)}\ T(\lambda)\ r(\lambda), \\ Y_f &= K \sum_{\lambda=380}^{780} E(\lambda)\ \overline{y(\lambda)}\ T(\lambda)\ r(\lambda), \\ Z_f &= K \sum_{\lambda=380}^{780} E(\lambda)\ \overline{z(\lambda)}\ T(\lambda)\ r(\lambda), \end{aligned} \tag{18}$$

where $T(\lambda)$ is spectral transmittance of the filter, X_f, Y_f, and Z_f are corresponding tristimulus values. Using the similar procedure as above, we can derive the final equations with matrix form as follows:

$$\begin{bmatrix} X_f \\ Y_f \\ Z_f \end{bmatrix} = \begin{bmatrix} \overline{X_f} \\ \overline{Y_f} \\ \overline{Z_f} \end{bmatrix} + \begin{bmatrix} X_{f1} & X_{f2} & X_{f3} & X_{f4} & X_{f5} & X_{f6} \\ Y_{f1} & Y_{f2} & Y_{f3} & Y_{f4} & Y_{f5} & Y_{f6} \\ Z_{f1} & Z_{f2} & Z_{f3} & Z_{f4} & Z_{f5} & Z_{f6} \end{bmatrix} \begin{bmatrix} \alpha_1 \\ \alpha_2 \\ \alpha_3 \\ \alpha_4 \\ \alpha_5 \\ \alpha_6 \end{bmatrix} \tag{19}$$

Combining Eqs. (17) and Eqs. (19), we have six independent equations with six unknown eigenvalues. The matrix form of these six equations is shown as follows:

$$\begin{bmatrix} X \\ Y \\ Z \\ X_f \\ Y_f \\ Z_f \end{bmatrix} = \begin{bmatrix} \overline{X} \\ \overline{Y} \\ \overline{Z} \\ \overline{X_f} \\ \overline{Y_f} \\ \overline{Z_f} \end{bmatrix} + \begin{bmatrix} X_1 & X_2 & X_3 & X_4 & X_5 & X_6 \\ Y_1 & Y_2 & Y_3 & Y_4 & Y_5 & Y_6 \\ Z_1 & Z_2 & Z_3 & Z_4 & Z_5 & Z_6 \\ X_{f1} & X_{f2} & X_{f3} & X_{f4} & X_{f5} & X_{f6} \\ Y_{f1} & Y_{f2} & Y_{f3} & Y_{f4} & Y_{f5} & Y_{f6} \\ Z_{f1} & Z_{f2} & Z_{f3} & Z_{f4} & Z_{f5} & Z_{f6} \end{bmatrix} \begin{bmatrix} \alpha_1 \\ \alpha_2 \\ \alpha_3 \\ \alpha_4 \\ \alpha_5 \\ \alpha_6 \end{bmatrix} \tag{20}$$

The eigenvalues are then give by:

$$\begin{bmatrix} \alpha_1 \\ \alpha_2 \\ \alpha_3 \\ \alpha_4 \\ \alpha_5 \\ \alpha_6 \end{bmatrix} = \begin{bmatrix} X_1 & X_2 & X_3 & X_4 & X_5 & X_6 \\ Y_1 & Y_2 & Y_3 & Y_4 & Y_5 & Y_6 \\ Z_1 & Z_2 & Z_3 & Z_4 & Z_5 & Z_6 \\ X_{f1} & X_{f2} & X_{f3} & X_{f4} & X_{f5} & X_{f6} \\ Y_{f1} & Y_{f2} & Y_{f3} & Y_{f4} & Y_{f5} & Y_{f6} \end{bmatrix}^{-1} \left(\begin{bmatrix} X \\ Y \\ Z \\ X_f \\ Y_f \end{bmatrix} - \begin{bmatrix} \overline{X} \\ \overline{Y} \\ \overline{Z} \\ \overline{X_f} \\ \overline{Y_f} \end{bmatrix} \right). \tag{21}$$

After determine the six eigenvalues, the spectral reflectance of human face can be obtained by basis functions using Eq. (5).

Now the question remaining is how we can connect the camera signals to tristimulus values. Most digital cameras have nonlinear photometric response that the relationship between the digital numbers in the image file and the scene reflectance which produced the digits is nonlinear. This relationship is known as the optoelectronic conversion function. The nonlinearity is employed to minimize visual artifacts caused by optical and digital limitations. To connect those digits to the tristimulus values, the digits should be first linearized based on the optoelectronic conversion function. The common methods are fit procedure using one-dimensional look-up table involving interpolation or a polynomial function and etc.

The next step is to transform linearized camera digits to tristimulus values. Since most digital cameras do not have spectral sensitivities that are linearly related to color-matching functions, a simple 3x3 transformation will yield considerable error. A common empirical technique recommended by Berns [17] is to include relative cumbersome square and covariance terms, or even higher order terms. The possible transform equation then could be written as

$$\begin{bmatrix} \hat{X} \\ \hat{Y} \\ \hat{Z} \end{bmatrix} = \mathbf{M} \begin{bmatrix} R \\ G \\ B \\ R^2 \\ G^2 \\ B^2 \\ RG \\ RB \\ GB \end{bmatrix} \tag{22}$$

where R, G and B are linearized digits of camera, $\hat{X}, \hat{Y}$ and $\hat{Z}$ are estimated tristimulus values, **M** is the transform matrix. The transform matrix M can be calculated from least square regression known as pseudoinverse method based on calibrated targets. The authors call this procedure as 2-step method that it first relates the digits to the tristimulus values using Eq. (22), then determine the eigenvalues using Eq. (21). However, least

square regression of **M** only minimizes the sum of square tristimulus errors; it has no guarantee to either provide minimum color difference or most accurate spectral fit. Therefore, to achieve the best accuracy of the final results, some necessary optimization should be performed to minimize the goal object which is of most important or interest. For example, the **M** matrix can be determined with the minimum average color difference or, in spectral image research, with the minimum root mean square error between estimated and measured spectra. It is worth noting that it works best to use different transform matrix for different sets of filters.

An alternative method is to establish the relationship between linearized digits and eigenvalues directly. This method is called a direct method. The form of digits chosen can be based on the Eqs. (21) and (22). The accuracy of 2-step method and direct method depends on certain situations; no one always works better than the other.

Imaging System Calibration

The portrait studio digital camera we used for this research is SONY DKC-ST5 Digital Photo Camera. It is a high-quality electronic photography system, using a three-chip high-resolution CCD camera with total 1,400,000 pixels. Its A/D conversion uses a 10-bit lookup table for each R, G and B channel, which makes flexible color gradation representation. The output image is 24-bit, 8-bit for each channel, with TIFF format. During the experiment, the camera automatic white balance was disabled by setting the temperature to 3200K for tungsten lighting we used. For signal-noise considering, we set the shutter speed to 1/1000 with the exposure of ISO160. We then employed a high quality white reference, barium sulfate coated paper, under the lighting and camera condition we would use for real image capturing, to adjust the camera setting so that the image of white reference would give maximum digit values without saturation and satisfy the white balance. The lighting system contained two lighting heads (Scanlite Digital 1000, Elinchrom) with Halogen Photo Optic lamps (FEL/1000w, 120V). The spectral radiance of the lighting on the position where real objects would be taken for pictures was measured by Spectroradiometer, SpectraScan 704 (PR-704), Photo Research Inc. The measured spectral radiance is given in Fig. 1 as follows:

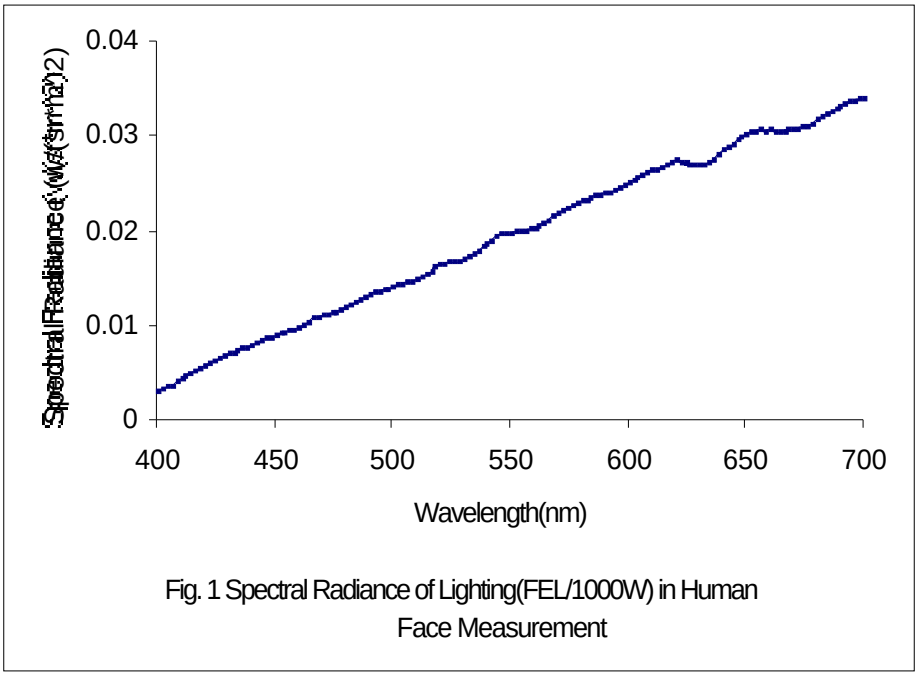

Fig. 1 Spectral Radiance of Lighting(FEL/1000W) in Human Face Measurement

Some necessary measurement and calibration should be performed before any serious experiment could be completed.

The first pre-experiment measurement was to measure the spectral sensitivity response of the camera. Two methods could be employed: monochromator method and interference filter method. Imai [7] showed that monochromator method is a better choice.

In monochromator method, a light source Module Model 740-20 (serial 8553) in connection with double monochromators, part of the Optical Radiation Measurement System Model 740A (serial 185268-5) from Optronic Laboratories Inc., would be used in this measurement. Hewlett Packard Hamsom 6274A DC Power Supply (0 – 60V 0 – 15A) is set to provide stable 0.06A current to the light. This light source with monochromator provided narrow-band illumination at the 10nm exit slit, over a range 380 – 780nm at 2nm intervals. The surface of the digital camera lens was kept to a proper distance from the exit slit of the monochromator. The images of the monochromator light were taken in a dark environment over the range of 380 – 780nm, in intervals of 2nm. Each image will be truncated in the same position centered in the light spot producing a proper, i.e., 106x33 pixels, 2-D image. The averaged digital counts for each channel over wavelength range then could be obtained. Next, the camera was replaced by a calibrated photo-detector (Optronic Laboratories Inc., OL730-5C Silicon Photo detector SIN:1152 Hex Key with calibration certification data: May 30, 1998) whose spectral responsivity was given and the source spectral irradiance was measured over the same range used

above by Optronic Laboratories Inc., Radiometer 730A (serial: 850190). Based on the average digital counts and the measured irradiance the spectral sensitivity of R, G, and B channels of the digital camera could be obtained. The relative spectral sensitivity of the camera is shown in the figure 2. The spectral sensitivity of the camera indicates that the wavelength response range of the camera is from 380nm to 700nm. Therefore, just as many researchers used, we will choose the wavelength range of 400nm to 700nm in our measurement. Since the PR704 can measure the spectra with the range from 380nm to 780nm with 2nm interval, all our spectral data will use interval of 2nm. The color matching function (CIE 1931, 2° observer), and other standard illumination spectra will then be interpolated 400nm to 700nm in interval of 2nm. It should be indicated that the spectral sensitivity of camera shown here is not exactly the same as we used for our real experiment. It was based on the setting after performing the white balance which was related to the lighting spectra shown in Fig. 1. Therefore, in Fig. 2, it is reasonable to understand that the blue channel is enhanced.

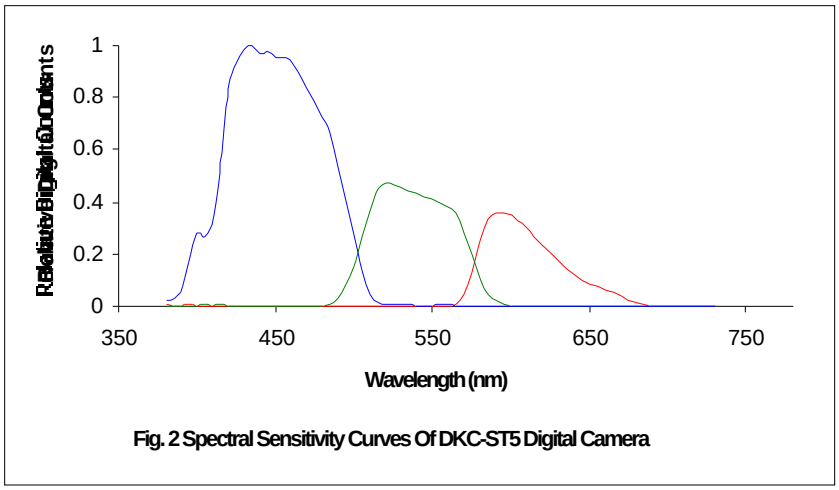

Fig. 2 Spectral Sensitivity Curves Of DKC-ST5 Digital Camera

With a wide-band filter attached to this camera, the imaging system will provide a multispectral image with total six wide-bands. The wide-band filter we selected for this research is 202 half C.T blue, Professional Lighting Filters, Bogen. Its spectral transmittance is shown in figure 3 which was measured using a Macbeth Color-Eye 7000, spectrophotometer.

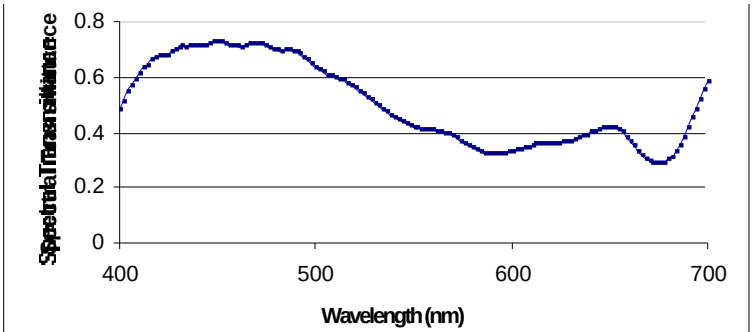

Fig. 3 Spectral Transmittance of Wide-band F

The criterion here is to choose a filter with some variation in spectral transmittance and the transmittance should not be too small in any wavelength[18]. Mathematically, the filter should provide three linear independent equations. Considering the fact that, generally, the blue channel image of CCD camera has relative low image-noise ratio, it is better to choose a filter with relatively high spectral transmittance in the short wavelengths. Figure 3 shows that the spectra have more absorption in long wavelengths than that in short wavelengths.

The next basic measurement was the optoelectronic conversion function (OECF) of the camera. The camera setting and imaging system was the same as we would perform for real imaging capturing. The OECF was determined by imaging gray scales, Kodak GrayScale, Q14, with the addition of a high quality white paper and a complete dark. Each gray scale was taken one image containing three R, G, B channel images. The images of gray scales should be all taken at the same position to avoid the non-uniform of the illumination involved. The camera system has a function to create a grid box with any size and any position shown on the screen of an attached monitor. Using this function, during measurement, each gray scale was easily placed at the same position shown by grid box which was located at the center of the image frame. For each gray scale, the digital count of image for each channel was a mean of the pixel values truncated at the center of the image with the pixel size of 31x41. The composite OECF of the camera is shown in figure 4.

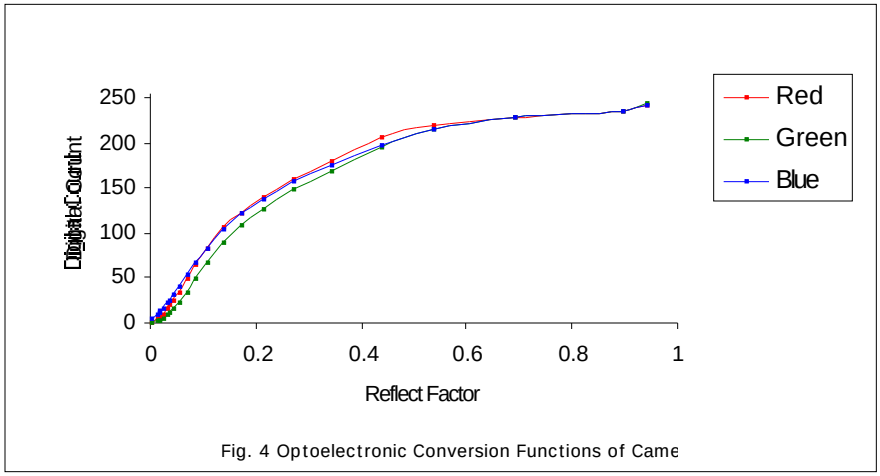

Fig. 4 Optoelectronic Conversion Functions of Came

The OECF curves are non-linear. After comparing with many fit methods, we find that three 1-D look-up tables will be a best choice to relate the digital counts to reflectance factors. As we mentioned in the previous section, the linearized R, G, B will be calculated based on OECF using these three 1-D look-up tables.

One difficult part of this research was to measure the spectral reflectance and its corresponding digital count (mean value) at the same position. We designed a system which includes an optical mirror and PR-704. We selected the circular aperture, setting of 0.5 degree, in PR-704 for the spectral measurement as illustrated in figure 5.

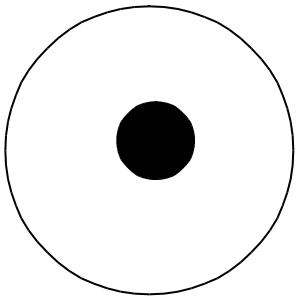

Fig. 5. Circular Aperture in PR-704

Optical radiation being measured passed through the aperture and then reached the detector for the light measurement. The mirror was attached to a slide mounted on carrier which could move along the table bench. This system was calibrated so that the pixel

positions in the image contributed to the light measurement in PR-704 were known. The distance between the object to PR-704 (distance from object to mirror plus distance from mirror to PR-704) was selected in such a way that the uncertainty of calibrated pixel area was less than 2.5% on the assumption that the object surface would move forth or back around the calibrated object position within 2cm. The distance we selected was about 1.6m. We could select a longer distance for accuracy purpose. However, the area covered by the aperture of PR-704 would be too large and the spectra measured would be averaged too much. The calibrated surface area of the object was an ellipse of height of about 0.73cm and width of about 0.75cm. During the experiment, we first took picture for the object, then moved the mirror to the calibrated position and made spectral measurement of the same object at the same position. The pixels of the image contributed to the spectral measurement could be truncated based on the calibrated pixel area and their mean digital count then could be obtained.

To measure the spectral reflectance of the mirror under the experimental condition, we first placed the white reference paper on the calibrated position where real objects would be taken for pictures and spectral measurement. Next, we measured the spectral radiance of that position with the mirror and PR-704 located at their calibrated positions. Then, we placed the PR-704 perpendicularly to the white reference paper, without mirror, with the same distance as that from PR-704 to mirror plus mirror to white paper at the previous step. Finally, we measured the spectral radiance at the same calibrated position where real objects would be taken for spectral measurement. Knowing the spectral reflectance of the white reference paper, the spectral reflectance of the mirror, therefore, could be easily calculated and is shown in figure 6.

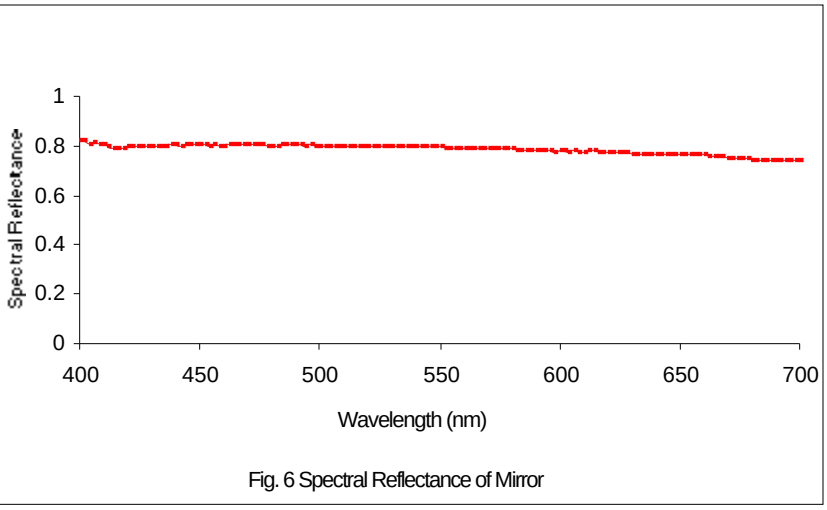

Fig. 6 Spectral Reflectance of Mirror

The picture of the main parts of imaging system is shown in figure 7.

Fig. 7 Picture main parts of imaging system

Experiment

It is worth indicating here that, for simple calculation purpose, we modified Eq. (5) avoiding the mean spectra term for all of our following calculations. The modified equation is given as follows:

$$\mathbf{r} = \mathbf{U} \cdot \alpha, \tag{23}$$

where **r** is an n×1 matrix of spectral reflectance utilizing n-point wavelength, **U** is an n×m matrix of m basis functions, and α is an m×1 matrix of eigenvalues.

We mentioned earlier that the number of bands or image channels used is dependent on the coverage percentage of the basis functions calculated from PCA. To get the first hand information about human face we applied spectrophotometer, Gretag SpectroScan, to directly measure spectral reflectance of the faces of four people, two from East Asia and two from America (Caucasian). This measurement obtained total 232 spectral reflectance of face including face skin, lips, eyes and hairs. Due to difficult measuring the spectral reflectance of eyes, eye data was based only on two people with successful measurement. The first three basis functions from PCA are shown in figure 8.

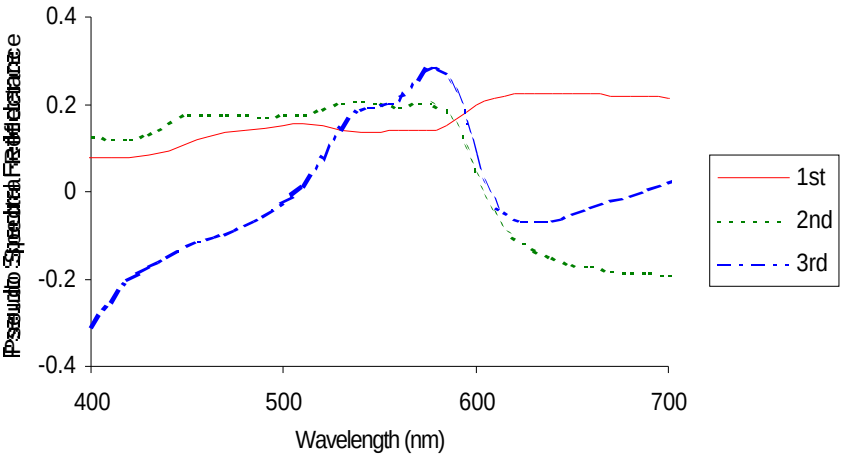

Fig. 8 First Three Basis Functions Of Faces in Direct Measurement

The coverage percentage of the first three basis functions is 99.80% while this number is 99.99 for the first six basis functions. This shows that the three basis functions can provide acceptably accurate results. As mentioned in the previous section, the spectral reflectance measured with real lighting and camera condition may involve different effect that will give some different results. Therefore, we decided to perform three wide band (without filter) and six wide band (with filter) spectral image experiments respectively.

A total of 16 people, nine Asian and seven American (Caucasian), participated in this experiment. For each person, we would select 16 different positions on the face for our

calibration purpose. We only restricted that those positions should include three on hairs, two on eyes, one on lips and the rest were on skin; their exact positions were not limited. The camera, spectroradiometer PR-704, and lighting in our imaging system were all calibrated and their relative positions could not be changed during the experiment. Therefore, we created a grid box, as mentioned earlier, on the image frame coincident with the position covered by aperture of PR-704 in spectral measurement. The objects were asked to adjust their chair up and down, left and right, until the position of interest fallen into the grid box shown on the monitor. They were asked to put their heads against the holder in the back and keep still during each measurement. For each position, one image without filter and one image with filter were taken, and the spectral measurement was then performed. The most difficult part was on the position of eyes that object was asked to keep eyes open, without blink, for about 30 seconds. For all objects, total 256 (16 x16) sets of measurement data were collected. We only employed 240 sets of data, from 15 people for system calibration and modeling. The rest of the data sets, 16 sets, from one person would be used for verification purposes.

Spectral Measurement Results

Based on the measured spectral radiance of the lighting, spectral reflectance of white paper and spectral reflectance of mirror, the spectral reflectance of the object could be obtained. Using the PCA method, the basis functions and their coverage percentages were calculated. The first six basis functions are shown in figure 9. The accumulative coverage percentages (ACP) for the first six basis functions are shown in table 1.

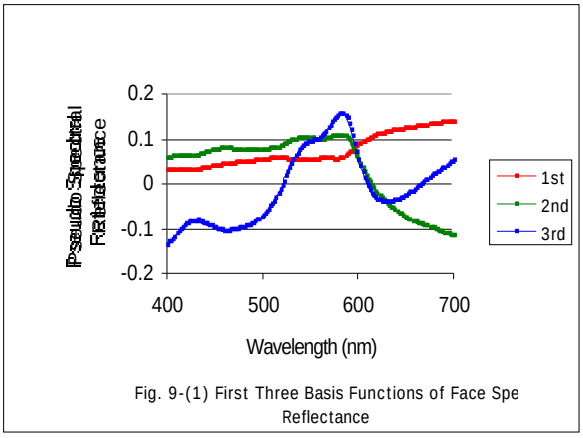

Fig. 9-(1) First Three Basis Functions of Face Spe
Reflectance

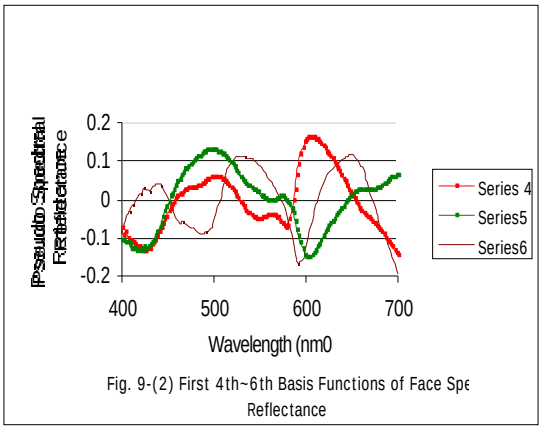

Fig. 9-(2) First 4th~6th Basis Functions of Face Spe
Reflectance

Fig. 9-(1) shows similar shape forms with that of Fig. 8. However, they show different shapes than those reported by Imai [8] whose results were only based on face skin. These differences are what we expected. Interesting thing is that, to achieve the 99.5% of the accumulative coverage percentage, our results only need first two basis functions while it required first three basis functions in Imai's work. This implies that our results have a more efficient representation considering that our data included more parts of spectral measurement. On the other hand, table 1 indicates that three basis functions can provide sufficient accuracy to describe the spectra in our experiment. Therefore, based on Eq. (20), image from regular three bands, i.e., R, G and B three channels, can be used to derive the spectral image with sufficient accuracy. However, due to the non-linearity of the OECF of the camera and non-linear relationship between camera spectral sensitivity and color matching functions, the procedure of transferring digital counts of the image to corresponding spectral reflectance will yield some extra error. Thus, in the following transform matrix determination, we will try both three channel and six channel spectral images. For comparison purpose, we also performed the PCA to face spectral reflectance of American people and Asian people separately. The first three basis functions for both groups of people are shown in figure 10 as follows:

Table 1. Accumulative coverage percentage of 1~ 6 basis functions.

basis functions	1	2	3	4	5	6
ACP(%)	98.15	99.55	99.92	99.97	99.98	99.99

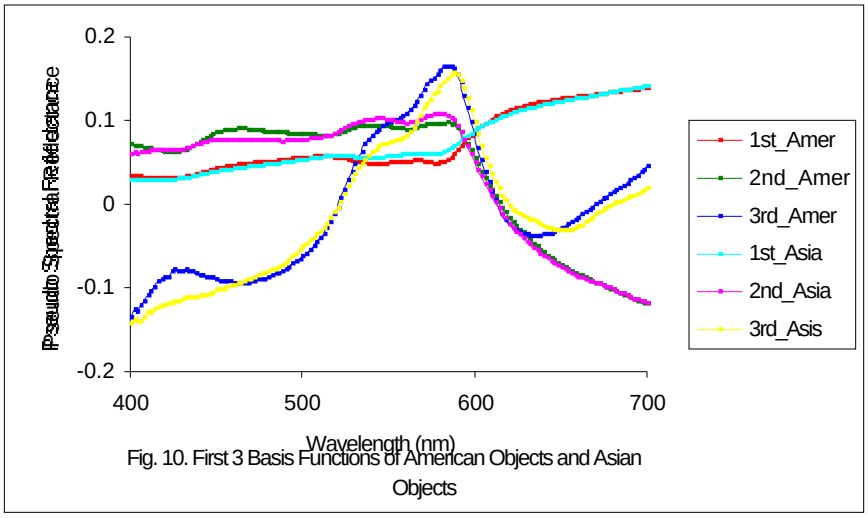

Fig. 10. First 3 Basis Functions of American Objects and Asian Objects

It is interesting to see that both groups show the very similar shapes of their basis functions.

Selection of Transform Matrix

As indicated in Eq. (5) ~ Eq. (22), we can use 2-step method and direct method to determine the transform matrix connecting linearized digital counts to tristimulus values or eigenvalues which can then be used to reconstruct the spectral reflectance. But first, the digital counts of the image pixels which contributed to the spectral reflectance measured need to be linearized based on OECF we obtained in basic measurement.

(1) **Linearized R, G and B values.**

We first transferred the original images, both without and with filter, to the reflectance factor space, pixel by pixel, based on the OECF. White correction was then required to be performed due to non-uniform illumination fallen on the objects. Compared to the depth dimensions of the objects, the distance from object to the camera could be regarded as infinity. Therefore, it was reasonable to assume here that the objects could be treated as flat objects. Thus, normal flat field procedure could be applied.

Then we truncated the pixels, which contributed to the spectral measurement, from the linearized image. The mean digital counts of those truncated pixels of red, green and blue channels were linearized R, G and B digital counts. For simple purpose, in the following sections we will use R, G and B notations to represent the linearized digital counts of red, green, and blue channel images, without using filter, respectively. The linearized digital counts from images using filter will be represented as R_f, G_f and B_f corresponding to red, green and blue channels respectively. The linearized digital counts were values between 0 to 1. The next step was to determine the transform matrix that could transfer the linearized digital counts to the eigvenvalues. Using the eigvenvalues and basis functions, the spectral reflectance could be constructed.

(2) **Transform Matrix**

For simple demonstration, we here define matrix **D** as follows:

$$\mathbf{D} = [\mathbf{D1} \quad \mathbf{D2} \quad \mathbf{D3} \quad \mathbf{I}],$$
$$\mathbf{D1} = [\mathbf{R} \quad \mathbf{G} \quad \mathbf{B}], \qquad \mathbf{D2} = [\mathbf{R}\ \mathbf{G} \quad \mathbf{R}\ \mathbf{B} \quad \mathbf{G}\ \mathbf{B} \quad \mathbf{R}^2 \quad \mathbf{G}^2 \quad \mathbf{B}^2], \tag{24}$$
$$\mathbf{D3} = [\mathbf{R}\ \mathbf{G}\ \mathbf{B} \quad \mathbf{R}^2\ \mathbf{G} \quad \mathbf{G} \quad \mathbf{B} \quad \mathbf{B}^2\ \mathbf{R} \quad \mathbf{R}^3 \quad \mathbf{G}^3 \quad \mathbf{B}^3].$$

where, $\mathbf{R}_{n,1}$, $\mathbf{G}_{n,1}$, and $\mathbf{B}_{n,1}$ are linearized digital count matrices with n = 240 as the number of data sets, $\mathbf{I}_{n,1}$ is the unit matrix for offset. Similar expressions can be written for matrix $\mathbf{D_f}$ as the case using filter. Therefore, **D** and $\mathbf{D_f}$ both contain 17 terms. We will use the expression **Q=[D**(n1: n2)] to represent that new matrix **Q,** a sub-matrix of **D,** containing column n1 to n2 of **D**. It is indicated here that we only used 238 real data sets and two data sets with very large calculation errors were rejected as measurement error.

As indicated in previous section, the least square regression using Eq. (22) may not give optimal spectral fit. Therefore, to determine the optimized transform matrix, we first, in 2 step method, applied Eq. (22) to obtain the least square result of transform matrix, **M**. Then using this M as an initial matrix, we performed optimization procedure to minimize the error of spectral estimation. The optimization criterion here is to minimize the root mean square of error between measured and estimated spectral reflectance. On the other hand, in direct method, the transform matrix is based on the spectra directly; matrix obtained from least square regression in direct method has already satisfied the minimizing of root mean square of error between spectra, measured and estimated. To demonstrate the spectral fit, the indices of metamerism were calculated using illuminations D50 and A. This calculation was employed Fairman's [17] metameric correction using parameric decomposition.

(i). Transform Matrix Using 3 Basis Function

We first tried the 2-step method using modified equation based on Eq. (22) with different terms of linearized digital counts. The modified equation is

$$\mathbf{XYZ} = \mathbf{M}\ \ \mathbf{Q}, \qquad (25)$$

where **XYZ** was an n×3 matrix of tristimulus values, **Q** was an n×m sub-matrix of **D**, and **M** was an m×3 transform matrix. We tried 7 terms, 11 terms and 17 terms of $\mathbf{D}'$ as shown in follows:

$$\begin{aligned} 7\,terms &: \ \mathbf{Q} = \left[\mathbf{D}(1:6)\ \ \mathbf{D}(17)\right] \\ 11\,term &: \ \mathbf{Q} = \left[\mathbf{D}(1:10)\quad \mathbf{D}(17)\right] \\ 17\,term &: \ \mathbf{Q} = \mathbf{D} \end{aligned} \qquad (26)$$

The transform matrix, **M**, based on least square regression can be expressed as follows:

$$\mathbf{M} = \mathbf{XYZ}\ \ \mathbf{Q}^T\ \ (\mathbf{Q}\ \ \mathbf{Q}^T)^{-1}, \qquad (27)$$

where $\mathbf{Q}^T$ is the transpose of **Q**. The results of regression and optimization are shown in table 2 as follows:

(a) 7 Terms Regression							(b) 7 Terms Checking					
	Without Optimization corr = 0.9955			With Optimization corr = 0.9957			Without Optimization Corr = 0.9968			With Optimization Corr = 0.9971		
	rms	meta-index	ΔElab	rms	meta-index	ΔElab	Rms	meta-index	ΔElab	rms	meta-index	ΔElab
mean	0.0110	0.83	1.89	0.0108	0.93	2.12	0.0125	0.62	1.55	0.0118	0.70	1.76
std.	0.0100	0.85	1.61	0.0098	1.01	1.85	0.0064	0.36	0.98	0.0066	0.40	0.98
max	0.0900	6.99	9.62	0.0908	8.06	10.64	0.0232	1.34	4.45	0.024	1.50	4.68
min	0.0016	0.03	0.11	0.0019	0.05	0.04	0.0032	0.11	0.40	0.0029	0.07	0.37

(c) 11 Terms Regression							(d) 11 Terms Checking					
	Without Optimization Corr = 0.9958			With Optimization Corr = 0.9959			Without Optimization Corr = 0.9965			With Optimization Corr = 0.9969		
	rms	meta-index	ΔElab	rms	meta-index	ΔElab	rms	meta-index	ΔElab	rms	meta-index	ΔElab
mean	0.0110	0.76	1.73	0.0106	0.84	1.93	0.0130	0.61	1.55	0.0119	0.66	1.75
std.	0.0095	0.76	1.49	0.0093	0.86	1.60	0.0066	0.32	1.00	0.0068	0.40	1.05
max	0.0840	6.5	9.13	0.0837	7.38	9.94	0.0238	1.44	4.58	0.0233	1.63	4.91
min	0.0012	0.062	0.25	0.0010	0.066	0.15	0.0040	0.14	0.21	0.0037	0.20	0.30

(e) 17 Terms Regression							(f) 17 Terms Checking					
	Without Optimization Corr = 0.9959			With Optimization Corr = 0.9961			Without Optimization Corr = 0.9959			With Optimization Corr = 0.9965		
	rms	meta-index	ΔElab	rms	meta-index	ΔElab	rms	meta-index	ΔElab	rms	meta-index	ΔElab
mean	0.0107	0.67	1.54	0.0104	0.75	1.74	0.0143	0.74	1.80	0.0132	0.71	1.79
std.	0.0094	0.62	1.34	0.0092	0.7	1.43	0.0072	0.39	0.82	0.0074	0.49	0.96
max	0.0820	0.54	7.66	0.0815	5.15	8.31	0.0255	1.92	4.08	0.0249	2.10	4.35
min	0.0010	0.054	0.12	0.0013	0.037	0.17	0.0040	0.25	0.64	0.0034	0.14	0.50

Table 2. Results in transform matrix determination using 3 basis functions with 2-step method.

where regression results were based on the data sets determining the transform matrix, results of checking were based on check data sets as mentioned early that were not involved in determining the transform matrix, rms values were root mean square error of spectra, meta-index were indices of metamerism, ΔElab were mean color difference, using CIELab, of the spectra, measured and estimated, using illumination D50, std. were standard deviations, and Corr were correlation values between spectra measured and estimated. The correlation and rms values in table 2 prove that the optimization did improve the spectral fit. However, the optimized transform matrix did not provide more accurate color reconstruction, except 17 terms for checking spectra, based on illuminant D50 and A.

The histograms of color difference between measured and estimated, using and without using optimization, for 7 and 17 term digital counts are shown in figure 11.

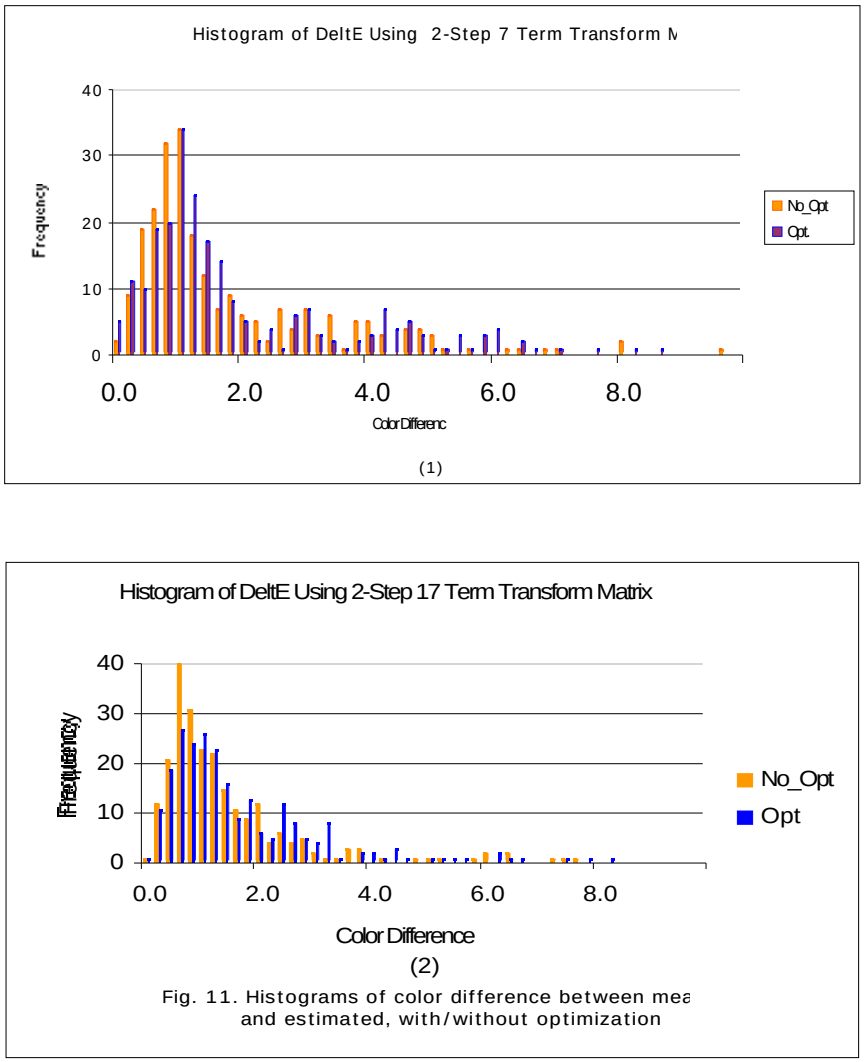

Fig. 11. Histograms of color difference between mea and estimated, with/without optimization

Histograms in Fig. 11 obviously shows that estimation without using optimization provided better color results. This implied that, to achieve more accurate color reproduction with certain illumination, it may be worth doing optimization to minimize the color difference. Table 2 and Fig. 11 also indicate that the overall reconstruction of color and spectra were more accurate when more terms of digital counts were used in Eq. (24). But this was not all true for checking data sets. The final selection of the transform matrix would also depend on the reconstructed results of the spectral image. We will discuss this in detail in the following section.

In a color system it is very important to know the direction of color error. Therefore, vector plots of a*b* results, measured and estimated with optimization, of the checking data sets are shown in figure 12.

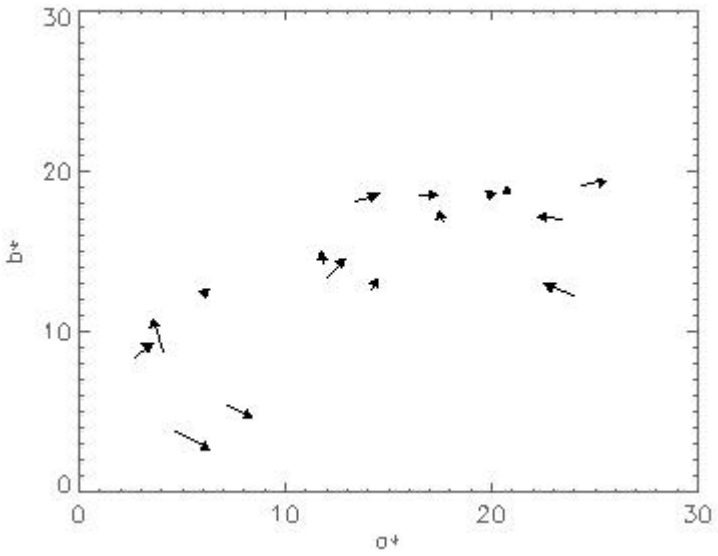

(1)

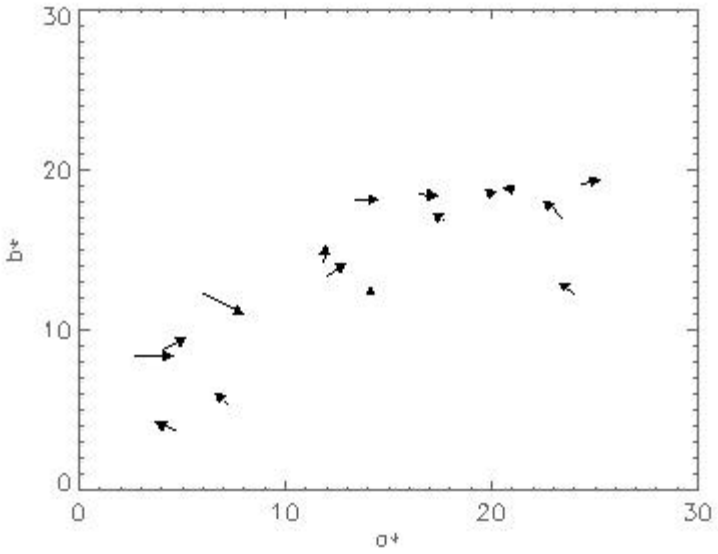

(2)

Fig. 12. Vector plot of a*b*.

The end of a tail indicates the a*b* position of the measured spectral reflectance.

The arrowhead indicates the a*b* position of the estimated spectral reflectance.

(1) Using 7 terms of digital counts. (2) Using 17 terms of digital counts.

Fig. 12 shows that, in some of the samples, high order transform matrix provided the better color accuracy while other samples provided better results with low order transform matrix. The vector plot also indicates that the arrows did not point toward the neutral axis (a*=b*=0). There was no obvious system error trend in regression using both 7 terms and 17 terms of **Q**.

We can also find the transform matrix using direct method. The equation for regression can be written as follows:

$$\mathbf{E} = \mathbf{Q}\ \ \mathbf{M}, \tag{28}$$

where **E** is an n×3 eigenvalue matrix obtained from PCA method, **Q** is an n×m matrix of linearized digital counts with m terms, and **M** is an m×3 transform matrix. Therefore, **M** can be determined using least square method as Eq. (29):

$$\mathbf{M} = (\mathbf{Q}\ \ \mathbf{Q}^T)^{-1}\ \ \mathbf{Q}^T\ \ \mathbf{E} \tag{29}$$

The results using 7 and 17 terms of **Q** are shown in table 3. Just for the purpose of saving pages, we do not show the results of using 11 terms of **Q** here.

(a). 7 Terms Regression							(b). 7 Terms Checking					
	Without Optimization Corr = 0.9957			With Optimization			Without Optimization Corr = 0.9971			With Optimization		
	rms	meta-index	Elab	rms	meta-index	Elab	rms	meta-index	Elab	rms	meta-index	Elab
Mean	0.0108	0.93	2.12	0.0108	0.93	2.12	0.0120	0.70	1.76	0.0120	0.70	1.76
std.	0.0098	1.01	1.84	0.0098	1.01	1.84	0.0066	0.40	0.98	0.0066	0.40	0.98
max	0.0910	8.01	10.7	0.0910	8.01	10.67	0.0240	1.50	4.68	0.0240	1.50	4.68
min	0.0019	0.041	0.05	0.0019	0.041	0.05	0.0029	0.07	0.37	0.0029	0.07	0.37

(c). 17 Terms Regression							(d). 17 Terms Checking					
	Without Optimization Corr = 0.9961			With Optimization			Without Optimization Corr = 0.9962			With Optimization		
	rms	meta-index	Elab	rms	meta-index	Elab	rms	meta-index	Elab	rms	meta-index	Elab
mean	0.0104	0.76	1.75	0.0104	0.76	1.75	0.0137	0.78	1.89	0.0137	0.78	1.89
std.	0.0092	0.69	1.41	0.0092	0.69	1.41	0.0075	0.57	1.07	0.0075	0.57	1.07
max	0.0800	5.09	8.07	0.0800	5.09	8.07	0.0250	2.38	4.73	0.0250	2.38	4.73
min	0.0010	0.013	0.17	0.0010	0.013	0.17	0.0034	0.17	0.52	0.0034	0.17	0.52

Table 3. Results of transform matrix regression with direct method using 3 basis functions

Table 3 shows that the direct method will give relatively larger error of regression results compared to that in 2-step method. This is because the eigenvalues estimated from PCA involved some error. The mean color difference, using D50, between spectra measured

and spectra reconstructed based on Eq. (5) using 3 basis functions was 0.09 with standard deviation of 0.06. Table 3 also shows that the regression results based on least square regression in Eq. (29) are the same as that based on minimizing the root mean square of spectra. The corresponding histograms of color difference between measured and estimated spectra are shown in figure 13. The vector plots of a*b* results of the checking data sets are shown in figure 14.

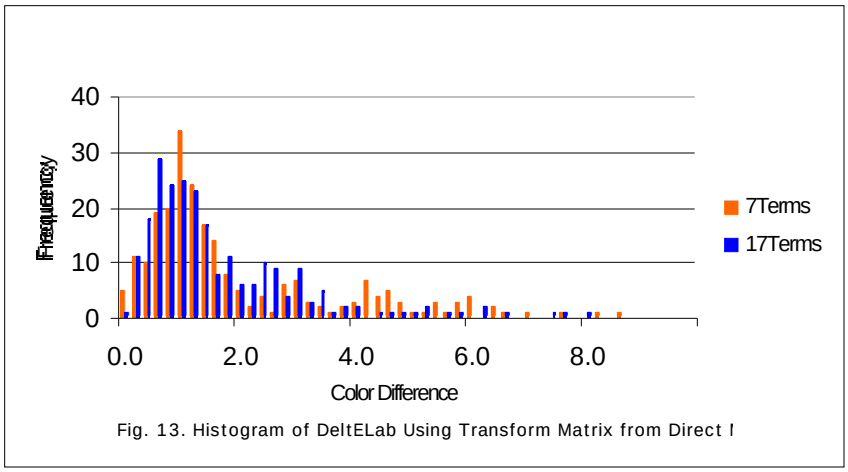

Fig. 13. Histogram of DeltELab Using Transform Matrix from Direct I

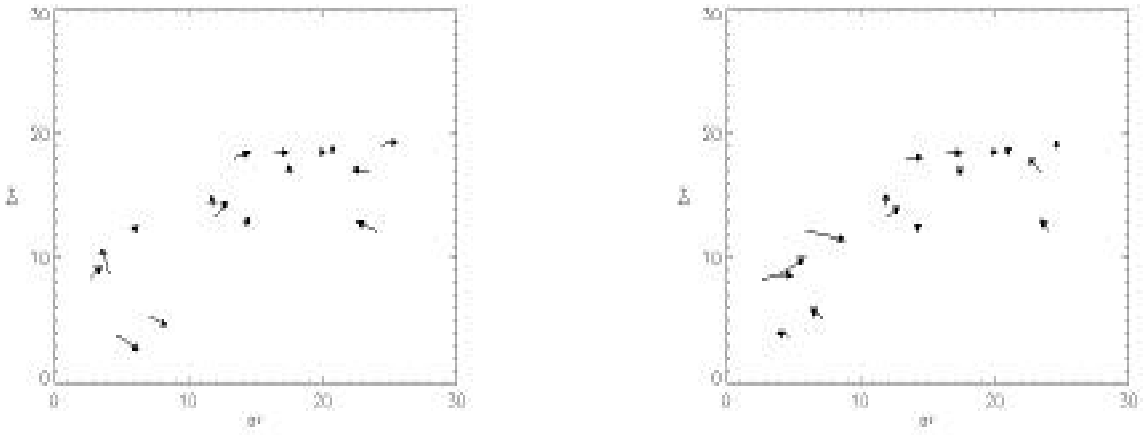

Fig. 14. Vector plots of a*b*.

The arrow notation is the same as in Fig. 12. (1). Using 7 terms; (2) Using 17 Terms.

The histogram and table 3 here also shows that the estimation of the overall color was better using higher order transform matrix. However, this is not true for checking data sets. The vector plots in Fig. 14 show that there were no obvious systematic error trends.

(ii). Transform Matrix Using 6 Basis Functions

We first tried 2-step method, but the results were too bad to be accepted. This may be due to the fact that the digital counts obtained from using filter were of relative low signal-to-noise ratio; relatively larger noises were involved in image using filter. Also, the relationships between tristimulus values and linearized digits without and with using filter were not the same. The latter may be more complicated than the former. Therefore, we here only show the results using direct method. Though equations used here are the same as Eqs. (28) and (29), some modifications have to be done to meet the application of 6 basis functions. **E** is now an n×6 eigenvalue matrix corresponding to 6 basis functions, and **M** is an m×6 transform matrix, **Q** is still an n×m matrix of linearized digital counts with m terms, but it need to include the digital counts from images using filter. We here only show 7 and 27 terms of **Q** which are redefined as follows:

$$\begin{aligned} 7\,terms: &\quad \mathbf{Q} = \left[\mathbf{D}(1:3) \quad \mathbf{D_f}(1:3) \quad \mathbf{I}\right] \\ 17\,terms: &\quad \mathbf{Q} = \left[\mathbf{D}(1:10) \quad \mathbf{D}(14:16) \quad \mathbf{D_f}(1:10) \quad \mathbf{D_f}(14:16) \quad \mathbf{I}\right] \end{aligned} \tag{30}$$

The results are shown in table 4.

(a). 7 Terms Regression							(b). 7 Terms Checking					
	Without Optimization Corr = 0.9960			With Optimization			Without Optimization Corr = 0.9963			With Optimization		
	rms	meta-index	Elab	rms	meta-index	Elab	rms	meta-index	Elab	rms	meta-index	Elab
mean	0.0100	0.75	1.71	0.0100	0.75	1.71	0.0130	0.66	1.53	0.0130	0.66	1.53
std.	0.0094	0.73	1.45	0.0094	0.73	1.45	0.0082	0.27	0.84	0.0082	0.27	0.84
max	0.0800	5.37	9.03	0.0800	5.37	9.03	0.0280	1.14	3.49	0.0280	1.14	3.49
(c). 17 Terms Regression							(d). 17 Terms Checking					
	Without Optimization Corr = 0.9968			With Optimization			Without Optimization Corr = 0.9963			With Optimization		
	rms	meta-index	Elab	rms	meta-index	Elab	rms	meta-index	Elab	rms	meta-index	Elab
mean	0.0091	0.60	1.39	0.0091	0.60	1.39	0.0125	0.67	1.74	0.0125	0.67	1.74
std.	0.0087	0.56	1.20	0.0087	0.56	1.20	0.0083	0.31	0.77	0.0083	0.31	0.77
max	0.0810	4.02	7.54	0.0810	4.02	7.54	0.0296	0.26	2.99	0.0296	0.26	2.99
min	0.0006	0.07	0.17	0.0006	0.07	0.17	0.0052	0.26	0.77	0.0052	0.26	0.77

Table 4. Results of Transform Matrix Regression with direct method using 6 Basis Function

Table 4 shows that regression using 7 terms of **Q** in 6 basis function application could provide more accurate results than that using 17 terms or 11 terms in 3 basis function application. However, the selection of transform matrix will also depend on the overall effect of reconstruction of spectral image. The histogram of color difference related to

regression using 7 terms of **Q** is shown in figure 15. The corresponding vector plot of a*b* of the checking data sets is shown in figure 16.

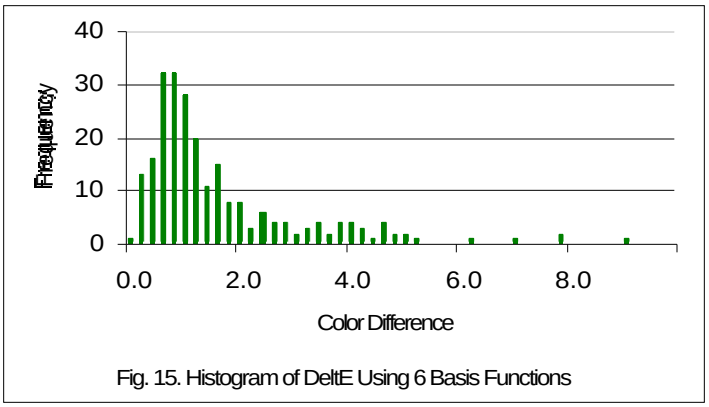

Fig. 15. Histogram of DeltE Using 6 Basis Functions

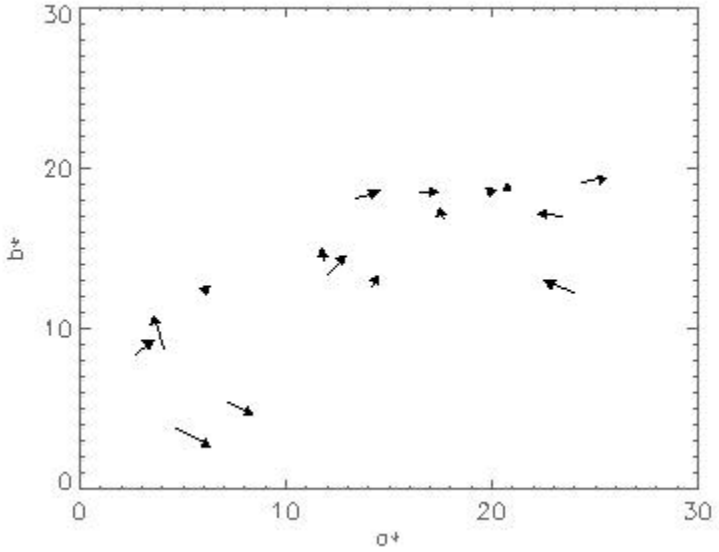

Fig. 16. Vector plot of a*b* using 6 basis functions

We have demonstrated the methods to determine the transform matrix. However, the matrices obtained above were based on limited number of measured samples. Different transform matrices based on different method, or based on same methods but using different terms of digital counts will have different flexibility to predict the overall estimation of spectral image. Therefore, it is worth performing reproduction of whole spectral image using different methods with different transform matrices obtained to test their overall accuracy and flexibility.

Reproduction of Spectral Image for Display

Applying the transform matrices obtained above, the spectral images, using either 3 or 6 basis functions, can be estimated, pixel by pixel, from the original R, G and B channel images. Each pixel of spectral image contains the eigenvalues which can be used to reconstruct the whole spectral reflectance, of this pixel, using Eq. (23). Therefore, once the illuminant spectra and observer are given, the tristimulus values of each pixel can be determined. Applying some color models, those tristimulus values will be transferred to digital counts of display device, i. e., monitor, for display. More complete and complex models can be found in the book written by Fairchild [20]. We selected relatively simple color models and straightforward procedure to achieve this. We will describe the procedure briefly as follows. All those transforms were processed pixel by pixel. When using 6 basis functions, the image registration procedure was required to be performed to two images obtained with and without using the filter before any transform could be performed.

We assumed that object was illuminated by illuminant D50 and the observer was 1931 standard observer. We also assumed that the display had a white point equal to the chromaticities of illuminant D65. The display environment had illumination close to D65. Therefore, we first applied the Bradford[21] chromatic adaptation transform to transfer the tristimulus values from illuminant D50 to illuminant D65. Then we used the sRGB[22] model to convert the tristimulus values, in illuminant D65, to display R, G and B values. Finally, we applied CRT characterization model [23] to transform the R, G and B values to digital counts which are values of 0~255. Those digital counts are final, reconstructed image values for display. Some mapping process may need to keep the transferred values within the device profiles. For more accurate display of reconstructed spectral image, the CRT need to be calibrated based on its colorimetric characterization[24].

By making a comparison between images displayed and real objects, we found the results as follows:

(1). When using three basis functions, either 2-step or direct method, the transform matrices with 17 terms were more flexible and would provide more accurate color reproduction than low order transform matrix did, especially the highlight in the eyes,

dark background and hairs. The matrices also predicted the colors of details very well. Moreover, the matrices could also predict colors of other materials, such as glasses, clothes, very well. It was not obviously that the transform matrix with 17 terms, using direct method, would yield little bit color shift, to blue, in the highlight of eyes. Meanwhile, transform matrix with 7 terms could not extrapolate colors very well; it failed to predict the highlight in the eyes. Compared to the reproduced image using transform matrix with 17 terms, reproduced images with 7 term transform matrix were looked little bit blurred. Considering the image noise, it was shown, though not obviously, that higher order transform matrix would yield little bit more image noise. This effect was also reported by Burns [25]. We then did a trial experiment by adding data sets of six gray targets of the Macbeth Color Checker into the original data sets to re-determine the transform matrix with 7 terms using 2-step method. The basis functions used were still the same as before. The purpose here was to enhance the flexibility of the transform matrix. The resulted display of reconstruction of spectral image was improved, especially the highlight in the eyes. The results of transform matrix regression added gray scale data sets are shown in table 5 as follows.

(a). 7 Terms Regression with Gray Scales							(b). 7 Terms Checking					
	Without Optimization Corr = 0.9944			With Optimization Corr = 0.9950			Without Optimization corr = 0.9964			With Optimization corr = 0.9968		
	rms	meta-index	Elab	rms	meta-index	Elab	rms	meta-index	Elab	rms	Meta-index	Elab
Mean	0.0120	0.87	1.9	0.0117	0.99	2.17	0.0130	0.62	1.59	0.0125	0.68	1.8
std.	0.0126	0.88	1.58	0.0116	1.08	1.85	0.0062	0.28	0.89	0.0063	0.29	0.95
max	0.1100	7.01	9.57	0.0930	8.21	10.71	0.0250	1.16	4.08	0.0230	1.37	4.54
min	0.0020	0.04	0.18	0.0024	0.03	0.18	0.0035	0.14	0.39	0.0037	0.17	0.44

Table 5. Results of transform matrix regression added six gray scale data sets.

Compared to the results in Table 2 with the same 7 terms of transform matrix, the accuracy of adding six gray scales was not affected very much. Therefore, to make low order transform matrix, i.e., 7 terms, more flexible, it is worth adding some data sets of gray scale targets. Nevertheless, in this research, high order transform matrices, though may yield relatively little bit more image noise, have benefit for more accuracy of color reproduction.

(3). When using 6 basis functions, the displayed image showed, obviously, that there were more image noises involved, especially in the image using higher order transform

matrix. Those image noises were mainly come from the original image using filter that caused relative low signal-noise ratio. This also implied that the image quality of the camera was not good enough for accurate multi-spectral image research. In addition, the effect of high order transform matrix on image noise was very obviously using 6 basis functions. However, it also showed that transform matrix with 7 terms could predict the color very well, either the highlight in the eyes, dark background, or color details in the face. Some samples of reconstructed spectral images for display are shown in figure 17. The printer is not calibrated.

Fig.17-(1). Reconstructed spectral images for displayed. Transform matrices were based on 3 basis functions, using 2-step method. The left images were calculated using 7 terms of **Q**, only face data sets were involved in determining the transform matrix. The middle images were calculated using 7 terms of **Q**, face data sets and six gray scale data sets were involved in determining the transform matrix. The right images were calculated using 17 terms of **Q**, and only face data sets were involved in determining the transform matrix.

Fig. 17-(2) Reconstructed spectral images for displayed. Transform matrices were based on 3 basis functions, using direct method. The left images were calculated using 7 terms of **Q**, only face data sets were involved in determining the transform matrix. The middle images were calculated using 7 terms of **Q**, using face data sets and six gray scale data sets in determining the transform matrix. The right images were calculated using 17 terms of **Q**, and only face data sets were involved in determining the transform matrix.

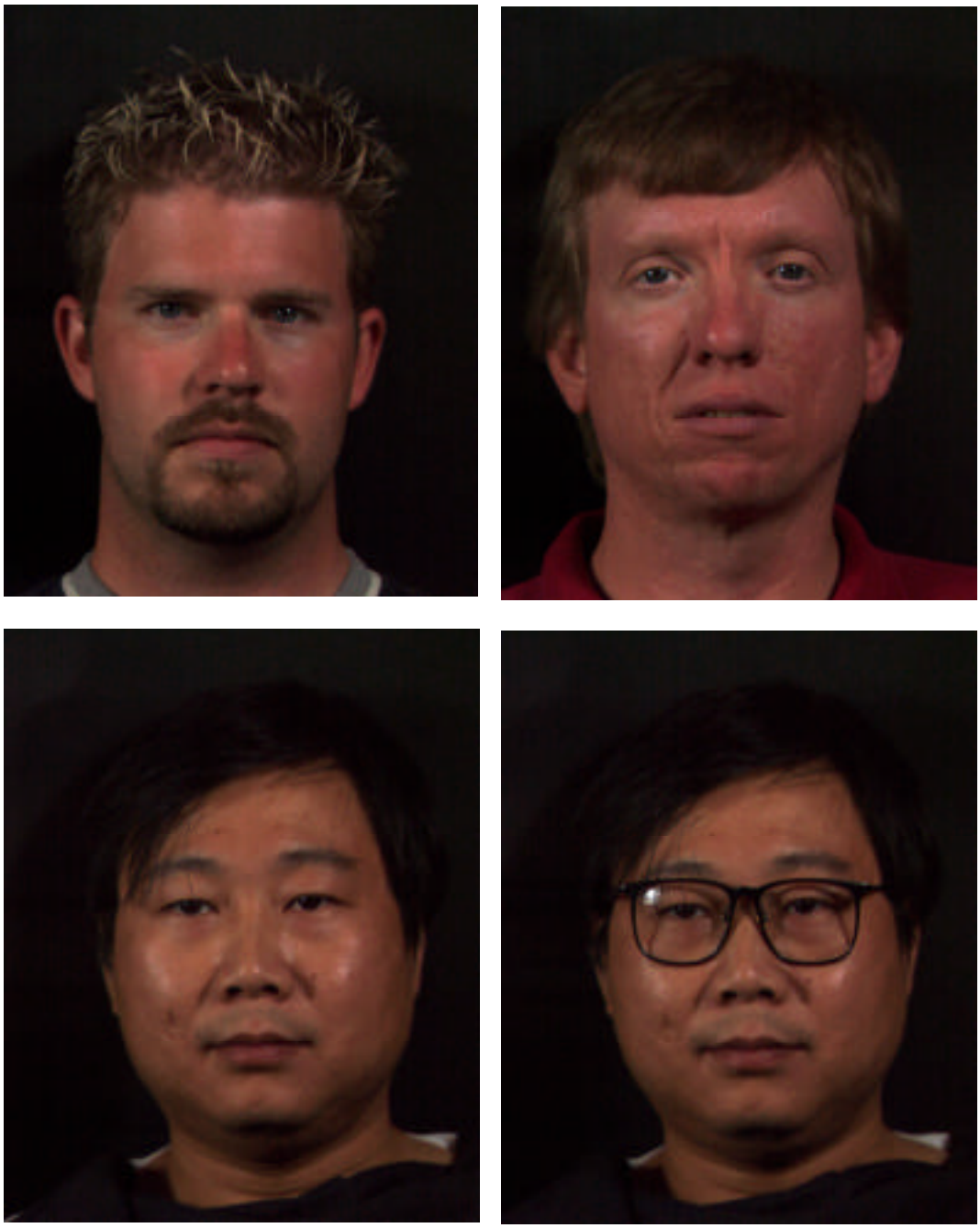

Fig. 17-(2) Reconstructed spectral images for displayed. Transform matrix was based on 6 basis functions, using direct method, 7 terms of **Q** and face data sets only.

Conclusion

A spectral imaging system calibrated directly from human objects has been accomplished. Based on PCA results of spectral reflectance of human face, including face skin, eyes, lips and hairs, three band and six band spectral images of human portraits have been successfully obtained. High order, 17 terms, transform matrices will provide more accurate, three band, spectral image with acceptable image noise. However, for six-band spectral image, transform matrix with low order of 7 terms will give most acceptable results. Due to the limit of image quality of the camera used, the 6-band spectral image did not meet the quality we originally expected. To obtain more accurate, multi-spectral image, a camera with high quality of image-noise and spectral sensitivities very close to color-matching functions is required. The obtained spectral image can be applied to color-imaging system design and analysis.

Acknowledge

The authors wish to express their thanks to Eastman Kodak Company for their financial support of this research. The authors also thank these individuals who participated in our experiment.

Reference

1. G.M. Johnson and M.D. Fairchild, Spectral Color Calculations in Realistic Image Synthesis, *IEEE Computer Graphics and Applications*, 19:4 47-53(1999).
2. R. S. Berns, Change for Color Science in Multimedia Imaging, in *Colour Imaging: Vision and Technology*, edited by L. MacDonald and M. R. Luo, John Wiley & Sons, Chichester, 99-127 (1998).
3. P. D. Burns and R. S. Berns, Analysis of Multispectral Image Capture, *Proceedings Fouth IS$T/SID Color Imaging Conference*, 19-22 (1996).
4. F. H. Imai and R. S. Berns, High-resolution Multi-spectral Image Archives – A Hybrid Approach, *Proceeding Sixth Color Imaging Conference: Color Science, System and Application*, 122 (1998).
5. R. S. Berns, F. H. Imai, P. D. Burns and Di-Y, Tzeng, Multi-spectral-based Color Reproduction Research at the Munsell Color Science Laboratory, *Proceeding of SPIE*, Europto Series**3409**, 14 (1998).
6. F. H. Imai and R. S. Berns, Spectral Estimation Using Trichromatic Digital Cameras, *Proceedings of the International Symposium on Multispectral Imaging and Color Reproduction for Digital Archives*, 42 (1999).

7. F. H. Imai, Multi-spectral Image Acquisition and Spectral Reconstruction using a Trichromatic Digital Camera System Associated with Absorption Filters, *Munsell Color Science Laboratory Technical Report*, http://www.cis.rit.edu/research/mcsl/pubs/PDFs/CameraReport.pdf (1998)
8. F. H. Imai, N. Tsumura, H. Haneishi and Y. Miyake, Principal Component Analysis of Skin Color and Its Application to Colorimetric Color Reproduction on CRT Display and Hardcopy, *Journal of Imaging Science and Technology*, **40**, No. 5, Sept./Oct., 422-430 (1996).
9. N. Ojima, H. Haneishi, and Y. Miyake, The appearance of Skin with Make-up(III)[Estimation for Spectral Reflectance of Skin with the HDTV Color Image], *J. SPSTJ*, **57**, 78-83 (1994).
10. Shoji Tominaga, Spectral Imaging by a Multi-Channel Camera, 38-47, *IS&T/SPIE Conference on Color Imaging: Device-Independent Color, Color Hardcopy and Graphic Arts IV,* San Jose, California (1999).
11. P. D. Burns, Aanlysis of Image Noise in Multi-Spectral Color Acquisition, *Ph.D. Thesis*, RIT (1997).
12. F. H. Imai and R. S. Berns, Spectral Estimation Using Trichromatic Digital Cameras, *International Symposium on Multispectral Imaging and Color Reproduction for Digital Archives, Proceedings*, 42-49, Chiba, Japan, October(1999)
13. P. D. Burns and R. S. Berns, Analysis multispectral image capture, *Proc. IS&T/SID 1995 Color Imaging Conference: Color Science, Systems and Applications*, 19-22(1996)
14. Di-Yuan Tzeng, Spectral-Based Color Separation Algorithm Development for Multiple-Ink Color Reproduction, *Ph.D. thesis*, Rochester Institute of Technology(1999)
15. R. A. Johnson, *Applied Multivariate Statistical Analysis*, 3rd Ed., Englewood Cliffs, N.J., Prentice Hall (1992).
16. A. C. Rencher, Method of Multivariate Analysis, *New York*, Wiley (1995).
17. R. S. Berns, Billmeyer and Saltzman's Principles of Color Technology, 3rd Edition, John Wiley & Sons (2000)
18. Person talk with F. H. Imai (2000).
19. H. S. Fairman, Metameric Correction Using Parameric Decomposition, *Color Res. Appl.*, **12**, 261-265 (1987).
20. M. D. Fairchild, Color Appearance Models, Addion Wesley Longman, Inc. (1997)
21. K. M. Lam, Metamerism and Colour Constancy, *Ph.D. Thesis*, University of Bradford (1985).
22. IEC 61966-3, Color Measurement and Management in Multimedia System and Equipment, Part 2-1: Colour Management¾ Default RGB Colour Space¾ sRGB, *International Electrotechnical Commission*, Geneva, Switzerland (1999).
23. R. S. Berns, R. J. Motta, and M. E. Dorzynski, CRT Colorimetry, Part I: Theory and Practice, *Color Res. Appl.*, **18**, 288-314 (1993).
24. R. S. Berns, Methods for Characterizing CRT Displays, *Displays*, **16**, 173-182 (1996).
25. P. D. Burns and R. S. Berns, Error Propagation Analysis for Color Measurement and Imaging, *Color Res. Appl.* **22**, 280-289 (1997).